



A NUMERICAL INVESTIGATION ON CONFINED IMPINGING ARRAY OF AIR JETS

Yücel ÖZMEN* ve Ertan BAYDAR**

*Karadeniz Teknik Üniversitesi Mühendislik Fakültesi Makina Mühendisliği Bölümü
61080 Trabzon, yozmen@ktu.edu.tr

** Karadeniz Teknik Üniversitesi Mühendislik Fakültesi Makina Mühendisliği Bölümü
61080 Trabzon, baydar@ktu.edu.tr

(Geliş Tarihi: 01. 07. 2011, Kabul Tarihi: 16. 04. 2012)

Abstract: The flow and heat transfer characteristics of two dimensional confined impinging array of air jets have been numerically investigated. Simulations have been carried out by using the Realizable k- ϵ and Standard k- ω turbulence models for Reynolds number of 30000, nozzles-to-plate spacing (H/D) in the range of 1-10 and jet-to-jet centerline spacing (S/D) in the range of 2-6. The effects of nozzle-to-plate spacing and jet-to-jet centerline spacing on the flow structure and heat transfer were examined. Calculated results show that the pressure coefficient and Nusselt number distributions of jet array impinging on a plate is strongly affected by the nozzle-to-plate spacing. On the other hand, the magnitudes of the local pressure coefficient and maximum Nusselt number at the central stagnation point is not affected by jet-to-jet spacing. When numerically obtained Nusselt number distributions compared with experimental data, it is seen that the Realizable k- ϵ turbulence model exhibits better agreement with the experimental data, compared to the Standard k- ω turbulence model for the investigated configurations.

Keywords: Subatmospheric region, Pressure coefficient, Nusselt distribution, Jet array, Turbulence models.

SINIRLANDIRILMIŞ ÇARPAN HAVA JETİ DİZİSİNİN SAYISAL İNCELENMESİ

Özet: Bu çalışmada, sınırlandırılmış çarpan hava jeti dizisinin oluşturduğu iki boyutlu akış alanında akış ve ısı transferi karakteristikleri sayısal olarak incelenmiştir. Sayısal çözümler, 1-10 lüle-levha açıklığı aralığında ve 2-6 jet merkezleri arası mesafe aralığında, Reynolds sayısının 30000 değeri için Realizable k- ϵ ve Standart k- ω türbülans modelleri ile elde edilmiştir. Lüle-levha açıklığı ve jetler arası mesafenin akış yapısı ve ısı transferi üzerindeki etkileri incelenmiştir. Çarpma levhası üzerindeki basınç katsayısı ve Nusselts sayısı dağılımlarının büyük ölçüde lüle levha açıklığından etkilendiği görülmüştür. Ayrıca, merkezi durma noktasında oluşan yerel basınç katsayısı ve maksimum Nusselt sayısı değerlerinin jetler arası mesafeden etkilenmediği belirlenmiştir. Realizable k- ϵ türbülans modeli ile elde edilen sonuçlar deneysel verilerle daha iyi bir uyum sergilemektedir.

Anahtar Kelimeler: Ortamaltı basınç bölgesi, Basınç katsayısı, Nusselt dağılımı, Jet dizisi, Türbülans modelleri.

NOMENCLATURE

C_p	Pressure coefficient [$\Delta P / (\rho U_o^2/2)$]	T	Temperature [K]
C_p	Specific heat at constant pressure [J/kgK]	T_w	Impingement wall temperature [K]
C_1, C_μ, C_2	Constants in the k- ϵ turbulence model	T_j	Jet exit temperature [K]
D	Nozzle diameter [m]	V_o	Nozzle exit velocity [m/s]
h	Convective heat transfer coefficient [W/m^2K]	u, v	Velocity components in z and r directions
H	Nozzle-to-plate spacing [m]	u_r	Friction velocity [m/s]
k	Turbulent kinetic energy [m^2/s^2]	z	Axial distance from the midpoint of the central jet [m]
k_a	Thermal conductivity of air [W/mK]	y^+	Dimensionless distance [$y^+=yu_r/v$]
L	Length of computational domain [m]	ν	Kinematic viscosity [m^2/s]
Nu	Nusselt number [$h \cdot D/k_a$]	ρ	Density of air [kg/m^3]
ΔP	Difference between the surface pressure and the atmospheric pressure [N/m^2]	β^*, β	Constants in the k- ω turbulence model
p	Pressure [N/m^2]	ϵ	Turbulent dissipation rate [m^2/s^3]
Q	Convective heat flux [W/m^2]	ω	Specific dissipation rate [1/s]
r	Radial distance from the midpoint of the central jet [m]	Φ	Viscosity loss function
Re	Nozzle Reynolds number [$U_o D/v$]	Γ	Exchange coefficient
S	Jet-to-jet centerline spacing [m], Source term	μ_{eff}	Effective viscosity
		μ	Laminar viscosity
		μ_t	Turbulent viscosity
		σ	Turbulent Prandtl number

INTRODUCTION

Impinging jets have been widely used in many industrial applications since they are effective tools to enhance and control heat and mass transfer. Applications include drying in paper industry, cooling and heating in food industry, annealing metallurgy, deicing of aircraft systems and cooling of heated components in gas turbine engines, computers and electronic instruments. A single air jet and an array of jets are used for different purposes. A single jet is usually employed to produce localized heating and cooling. In many applications, a large surface area is required to be heated or cooled, or enhancement of global heat transfer is needed. In such cases the interaction between the jets in the array plays an important role in the cooling performance. Thus, it is necessary to apply multiple-jet system (Hollworth and Berry, 1978).

There is a considerable body of literature dealing with flow and the heat transfer in array of jets (Metzger *et al.*, 1979; Hollworth and Dagan, 1989; Kim and Benson, 1993; Barata, 1996; Garrett and Webb, 1999; Tzeng *et al.*, 1999; Miao *et al.*, 2009). These investigations have focused largely on arrays for which cross-flow effects degrade high stagnation heat transfer and the effect of geometric arrangement of jets. Martin (1977) and Polat *et al.* (1989) reviewed the heat transfer characteristics of multiple impinging air jets without cross-flow. Koopman and Sparrow (1976) noted that there are two types of interaction between the jets in the multiple-jets system. The first type was the interaction between adjacent jets prior to impingement on the surface. The second type was the collision of two wall jets, which were generated after impingement. Such collision became significantly important when the jets were closely spaced, the nozzle-to-plate spacing was small, and the jet velocity is high. Koopman (1975) obtained high heat transfer coefficients for multiple jets in the stagnation region and at the second stagnation point (the midpoint between the two neighboring jets). The fluid flow and heat transfer characteristics of multiple impinging slot jets with an inclined confinement surface was studied by Yang and Shyu (1998). Their results show that the maximum local Nusselt number and maximum pressure on the impingement surface move downstream while the inclination angle was increased. Huber and Viskanta (1994) have examined the influence of spent air exits located between the jets on local heat transfer coefficient for a confined impinging array of air jets. Saad *et al.* (1992) compared the turbulence, mean flow and heat transfer characteristics of an array of confined impinging slot jet with those of a single jet. Tanaka (1974) found that a particular feature of the two-dimensional parallel flow of double jets was the appearance of a sub-atmospheric region between the jets, owing to the entrainment of the fluid by the turbulent jet. Fattah (2007) noted that a sub atmospheric region occurs on the impingement plate and its effect decreases with increasing nozzle-to-plate spacing at the

impinging circular twin-jet flow. Mikhail *et al.* (1982) explained that the average Nusselt number of the double jets system increased with decreasing jet-to-jet spacing. Fernandez *et al.* (2007) investigated numerically the flow field of a turbulent twin plane jet impinging normally onto a flat surface by using Standard k- ϵ , Realizable k- ϵ and Standard k- ω turbulence models and concluded that none of the turbulence models correctly predicts the flow in the impact region. Dagtekin and Oztop (2008) carried out a numerical investigation to examine the effect of Reynolds number, bottom-wall spacing and the distance between two jets on heat transfer and fluid flow. They reported that multi-cellular flow is formed in the impingement region due to the interaction between two jets. The flow and heat transfer characteristics of impinging laminar square twin jets have been numerically investigated by Aldabbagh and Sezai (2002). The calculated results show that the flow structure of square twin jets impinging on a heated plate is strongly affected by the jet-to-plate distance. A two dimensional numerical model was used by Chuang *et al.* (1992) to determine the flow characteristics associated with an unsteady, compressible impinging twin slot jet between two plates. The calculated results show that several recirculating zones are distributed around the flow field. In addition, a fountain upwash flow occurs between the nozzles, and two low-pressure recirculating zones are induced by the interaction between the nozzle mainstream and the fountain upwash flow. The three dimensional turbulent impinging square twin-jets with no cross flow is analyzed by Chuang and Nieh (2000) using PHOENICS code. The calculated results show that the size and location of the recirculating zones around the jets are different from the two dimensional flow fields due to the effect of stretching in the transverse direction. Seyedein *et al.* (1995) used the numerical method to simulate the two dimensional turbulent flow and heat transfer from confined multiple impinging slot jets. Xing *et al.* (2010) conducted a combined experimental and numerical investigation of the heat transfer characteristics within an array of impinging jets. Kumar and Prasad (2011) investigated flow and heat transfer of multiple circular jets impinging on a flat surface with effusion.

Jets array impingement on the target plate and interaction between pairs of adjacent jets are very complicated phenomena. To approach these phenomena using theoretical analysis and experimental measurements can be quite difficult. The cost of the experimentation may be substantial in order to understand the structure of the impinging jet arrays. Therefore, numerical simulation may be a cost effective approach to the investigation of array of air jets. The present study is concerned with the numerical investigation of the confined impinging jet array flow fields. Two low cost turbulence models were used to simulate the strong turbulence and heat transfer of impinging jet array. The effect of jet flow parameters, such as nozzle-to-plate spacing and jet-to-jet centerline spacing, and resulting flow parameters including surface

pressure distributions and Nusselt distributions were examined for Reynolds number of 30000, the nozzle-to-plate spacings of 1-10 and jet-to-jet centerline spacings of 2-6. The main aim of the study is to investigate the relative performance of turbulence models in predicting two dimensional turbulent flow and heat transfer from confined impinging jet array. The second aim is to study the effect of the interaction between the jets on the flow structure and to investigate the effect of subatmospheric regions on the local heat transfer.

NUMERICAL STUDY

Mathematical Model

In the present study, it is assumed that the air flow is turbulent, steady-state and Newtonian with temperature-dependent fluid properties. A numerical solution of the mean flow and thermal fields requires resolving the Reynolds averaged Navier-Stokes equations and time averaged energy equations. These equations for two dimensional, incompressible and continuity flow in cylindrical coordinates can be written as given below,

mass continuity:

$$\frac{\partial}{\partial z}(\rho u) + \frac{1}{r} \frac{\partial}{\partial r}(r \rho v) = 0 \quad (1)$$

z-momentum:

$$\begin{aligned} \frac{\partial}{\partial z}(\rho u u) + \frac{1}{r} \frac{\partial}{\partial r}(r \rho v u) = -\frac{\partial p}{\partial z} + \frac{\partial}{\partial z} \left(\mu_{eff} \frac{\partial u}{\partial z} \right) \\ + \frac{1}{r} \frac{\partial}{\partial r} \left(r \mu_{eff} \frac{\partial u}{\partial r} \right) + S^u \end{aligned} \quad (2)$$

r-momentum:

$$\begin{aligned} \frac{\partial}{\partial z}(\rho u v) + \frac{1}{r} \frac{\partial}{\partial r}(r \rho v v) = -\frac{\partial p}{\partial r} + \frac{\partial}{\partial z} \left(\mu_{eff} \frac{\partial v}{\partial z} \right) \\ + \frac{1}{r} \frac{\partial}{\partial r} \left(r \mu_{eff} \frac{\partial v}{\partial r} \right) + S^v \end{aligned} \quad (3)$$

energy:

$$\begin{aligned} \rho C_p \left(u \frac{\partial T}{\partial z} + v \frac{\partial T}{\partial r} \right) = k \left[\left(\frac{\partial^2 T}{\partial z^2} \right) + \left(\frac{1}{r} \frac{\partial}{\partial r} \left(r \frac{\partial T}{\partial r} \right) \right) \right] \\ + \mu \Phi \end{aligned} \quad (4)$$

Where S^u and S^v represent the source terms and Φ is viscous loss function and they are given by the following expressions

$$S^u = \frac{\partial}{\partial z} \left(\mu_{eff} \frac{\partial u}{\partial z} \right) + \frac{1}{r} \frac{\partial}{\partial r} \left(\mu_{eff} r \frac{\partial v}{\partial r} \right) \quad (5)$$

$$\begin{aligned} S^v = \frac{\partial}{\partial z} \left(\mu_{eff} \frac{\partial u}{\partial r} \right) + \frac{1}{r} \frac{\partial}{\partial r} \left(\mu_{eff} r \frac{\partial v}{\partial r} \right) \\ - 2 \mu_{eff} \frac{v}{r^2} \end{aligned} \quad (6)$$

$$\Phi = \left\{ 2 \left[\left(\frac{\partial v}{\partial r} \right)^2 + \left(\frac{v}{r} \right)^2 + \left(\frac{\partial u}{\partial z} \right)^2 \right] + \left(\frac{\partial v}{\partial z} + \frac{\partial u}{\partial r} \right)^2 - \frac{2}{3} (\nabla \cdot v)^2 \right\} \quad (7)$$

Numerical solutions have been performed by using Realizable k- ϵ and Standard k- ω turbulence models. The turbulence models with two equations employ the Boussinesq approximation to relate the Reynolds stresses to the mean velocity gradients. Realizable k- ϵ model gives an approach about normal stress related to physics of turbulent flow to eliminate some mathematical constrains. In the Realizable k- ϵ , the turbulent kinetic energy (k) and its dissipation rate (ϵ) are computed from the following equations:

turbulence kinetic energy:

$$\begin{aligned} \frac{\partial}{\partial z}(\rho u k) + \frac{1}{r} \frac{\partial}{\partial r}(r \rho v k) = \frac{\partial}{\partial z} \left(\Gamma_k \frac{\partial k}{\partial z} \right) + \\ \frac{1}{r} \frac{\partial}{\partial r} \left(r \Gamma_k \frac{\partial k}{\partial r} \right) + S^k \end{aligned} \quad (8)$$

turbulence dissipation rate:

$$\begin{aligned} \frac{\partial}{\partial z}(\rho u \epsilon) + \frac{1}{r} \frac{\partial}{\partial r}(r \rho v \epsilon) = \frac{\partial}{\partial z} \left(\Gamma_\epsilon \frac{\partial \epsilon}{\partial z} \right) + \\ \frac{1}{r} \frac{\partial}{\partial r} \left(r \Gamma_\epsilon \frac{\partial \epsilon}{\partial r} \right) + S^\epsilon \end{aligned} \quad (9)$$

In the above equations, u and v represent the axial (z) and radial (r) components of the velocity vector, ρ denotes fluid density, and μ_{eff} is the effective viscosity for momentum transport given by

$$\mu_{eff} = \mu + \mu_t \quad (10)$$

Where μ is the molecular viscosity and μ_t is the ‘‘turbulent’’ viscosity given by the relation

$$\mu_t = C_\mu \rho k^2 / \epsilon \quad (11)$$

The effective exchange coefficients in the equations for k and ϵ are given by

$$\Gamma_k = \mu + \frac{\mu_t}{\sigma_k} \quad (12)$$

$$\Gamma_\epsilon = \mu + \frac{\mu_t}{\sigma_\epsilon} \quad (13)$$

Where σ_k and σ_ε are the turbulent Prandtl/Schmidt numbers. S^k and S^ε represent source terms for k and ε and they are given by the following expressions

$$S^k = \mu_t \left[2 \left\{ \left(\frac{\partial u}{\partial z} \right)^2 + \left(\frac{\partial v}{\partial r} \right)^2 + \left(\frac{v}{r} \right)^2 \right\} + \left(\frac{\partial v}{\partial z} + \frac{\partial u}{\partial r} \right)^2 \right] - \rho \varepsilon \quad (14)$$

$$S^\varepsilon = C_1 \frac{\varepsilon}{k} \mu_t \left[2 \left\{ \left(\frac{\partial u}{\partial z} \right)^2 + \left(\frac{\partial v}{\partial r} \right)^2 + \left(\frac{v}{r} \right)^2 \right\} + \left(\frac{\partial v}{\partial z} + \frac{\partial u}{\partial r} \right)^2 \right] - C_2 \rho \frac{\varepsilon^2}{k} \quad (15)$$

The standard values for constant are used: $C_1=1.44$, $C_2=1.9$, $C_\mu=0.09$, $\sigma_k=1.0$, $\sigma_\varepsilon=1.2$.

The Standard k - ω model is based on the transport equations of turbulent kinetic energy (k) and of specific dissipation rate ($\omega=\varepsilon/k$). The transport equations for k and ω are:

turbulence kinetic energy:

$$\frac{\partial}{\partial z} (\rho u k) + \frac{1}{r} \frac{\partial}{\partial r} (r \rho v k) = \frac{\partial}{\partial z} \left(\Gamma_k \frac{\partial k}{\partial z} \right) + \frac{1}{r} \frac{\partial}{\partial r} \left(r \Gamma_k \frac{\partial k}{\partial r} \right) + S^k \quad (16)$$

specific dissipation rate:

$$\frac{\partial}{\partial z} (\rho u \omega) + \frac{1}{r} \frac{\partial}{\partial r} (r \rho v \omega) = \frac{\partial}{\partial z} \left(\Gamma_\omega \frac{\partial \omega}{\partial z} \right) + \frac{1}{r} \frac{\partial}{\partial r} \left(r \Gamma_\omega \frac{\partial \omega}{\partial r} \right) + S^\omega \quad (17)$$

Turbulent viscosity at this model is given by

$$\mu_t = \frac{\rho k}{\omega} \quad (18)$$

The effective exchange coefficients in the equations for k and ω are given by

$$\Gamma_k = \mu + \frac{\mu_t}{\sigma_k} \quad (19)$$

$$\Gamma_\omega = \mu + \frac{\mu_t}{\sigma_\omega} \quad (20)$$

For this case, the turbulent Prandtl/Schmidt numbers are $\sigma_k = \sigma_\omega = 2.0$. S^k and S^ω represent source terms for k and ω and they are given by the following expressions

$$S^k = \mu_t \left[2 \left\{ \left(\frac{\partial u}{\partial z} \right)^2 + \left(\frac{\partial v}{\partial r} \right)^2 + \left(\frac{v}{r} \right)^2 \right\} + \left(\frac{\partial v}{\partial z} + \frac{\partial u}{\partial r} \right)^2 \right] - \beta^* \rho k \omega \quad (21)$$

$$S^\omega = \frac{\omega}{k} \mu_t \left[\left\{ \left(\frac{\partial u}{\partial z} \right)^2 + \left(\frac{\partial v}{\partial r} \right)^2 + \left(\frac{v}{r} \right)^2 \right\} + \left(\frac{\partial v}{\partial z} + \frac{\partial u}{\partial r} \right)^2 \right] - \beta \rho \omega^2 \quad (22)$$

The standard values for constant are used: $\beta^*=0.09$ and $\beta=0.072$.

Flow Field and Boundary Conditions

A schematic of the jet array configuration and computational domain is shown in Figure 1 where the flow field, the main dimensions and the prescribed boundary conditions are specified. Three strong main jets are injected through upward from the nozzles of diameter $D=25$ mm with a velocity V_0 and induced the surrounding flow to enter the flow field. The flow direction of the fluid is spread in to the surrounding when the array of air jets impinges perpendicularly on a plate at a distance H from the nozzles. S represents the jet-to-jet centerline spacing. The length of computational domain in the x -direction is approximately $L=30D$. The following boundary conditions were used: the impingement plate was specified as an isothermal wall and constant temperature condition are used as $T_w = 323$ K, jet exit temperature was taken as constant temperature of $T_j = 300$ K which was equal to confinement plate temperature and no-slip condition were specified on every wall; the mean velocity and turbulence profiles measured at the nozzles exit were used as velocity inlet conditions of computational domain and pressure outlet boundary conditions were assumed at outlet planes.

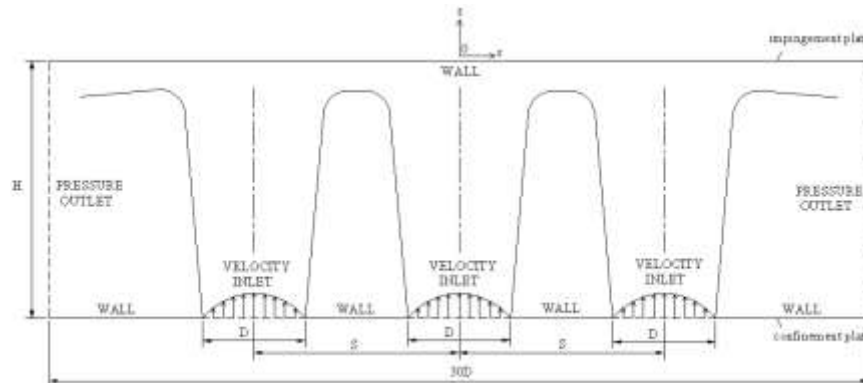


Figure 1. Schematic of the jet array configuration and computational domain.

Numerical Solution Procedure

The governing equations were solved using the FLUENT 6.3.26 software, by finite volume discretization, using a segregated solver with an implicit formulation. For the 2D simulations the diffusion and convective terms in the equations were approximated by second order upwind scheme. The discretized equations for the pressure-velocity coupling were solved by using the SIMPLEC algorithm on staggered grids. SIMPLEC procedure uses modified equation for face flux correction. The use of modified correction equation accelerates convergence. Pressure was solved using standard discretization scheme. A second order discretization method was used for the other variables (momentum, turbulent kinetic energy, turbulence dissipation rate and energy equation). Second order discretization scheme presents higher-order accuracy especially for complex flows involving separation. Enhancement wall treatment was used as wall function to obtain reasonably accurate predictions near the wall. Enhanced wall treatment is a near-wall modeling method that combines a two-layer model with enhanced wall functions. The two-layer approach is an integral part of the enhanced wall treatment and is used to specify the turbulent viscosity in the near-wall cells. In this approach, the whole domain is subdivided into a viscosity-affected region and a fully-turbulent region. Thus, more accurate results are obtained near the wall. The convergence criterion for the residuals was set to 1×10^{-6} for all dependent variables. To ensure the attainment of grid-independent results, sensitivities of both grid numbers and grid distributions were tested for each case. The mesh used is refined for each value of H/D and S/D until negligible differences are obtained. Finer computational grids were set near the wall and y^+ was less than 2.5. Refined grid density of 200×60 (12000 cells) in the whole computational domain is sufficient. The overall discretization uncertainty was estimated to be below 5 %.

RESULTS AND DISCUSSION

Numerical simulations were carried out for the nozzle-to-plate spacings (H/D) of 1-10, jet-to-jet centerline spacings (S/D) of 2-6 and the Reynolds number of 30000 for the confined impinging jet array. Computations were performed by using Realizable $k-\epsilon$ and Standard $k-\omega$ turbulence models.

Flow Structure

Flow field images obtained with two turbulence models at $Re=30000$ and $S/D=4$ for $H/D=1, 3, 6$ and 10 are given in Figure 2 and Figure 3. Figures 2a-d show the streamlines of the computed velocity fields with Realizable $k-\epsilon$ turbulence model. As soon as the jets exit from the nozzles, the fluid is dragged radially towards the jets from the surrounding. As a result toroidal vortices are formed around each of the jets. The peripheral vortices around the central jet are divided in

two co-rotating vortices. At lower nozzle-to-plate spacings, the wall jets fill the almost whole gap between the plates. Recirculation regions occur at the both sides of the central jet and at the outward of the other neighbor jets. The size of the recirculation regions increases with increasing H/D . After central jet impinges on the impingement plate, it spreads radially outward along the wall. This behavior of the central jet suppresses the motion of neighbor jets in the axial direction and causes their orientation radially outward without impinging on the impingement plate. As H/D spacing increases, vortices occurring outward of the neighbor jets get closer to the impingement plate. Similar findings are also reported by Aldabbagh and Sezai (2002). Streamlines of the computed velocity fields for the same nozzle-to-plate spacings with Standard $k-\omega$ turbulence model are shown in Figures 3a-d. Contrary to the Realizable $k-\epsilon$ turbulence model results, the size of vortex pairs decreases with increasing H/D for the Standard $k-\omega$ turbulence model. Although the velocity fields computed for both Realizable $k-\epsilon$ and Standard $k-\omega$ turbulence models are similar, the size of recirculation regions computed using Standard $k-\omega$ turbulence model is small. Figures 4a-c illustrate the streamline images obtained with Realizable $k-\epsilon$ turbulence model at $H/D=3$ and $Re=30000$ for $S/D=2, 4$ and 6 . It is seen that the sizes of co-rotating vortices occurred between the two jets increase with increasing S/D . Figures 5a-c show the streamline images obtained with Standard $k-\omega$ turbulence model at $H/D=3$ and $Re=30000$ for $S/D=2, 4$ and 6 . As in Figures 4a-c, the size of vortex pairs increases with increasing S/D .

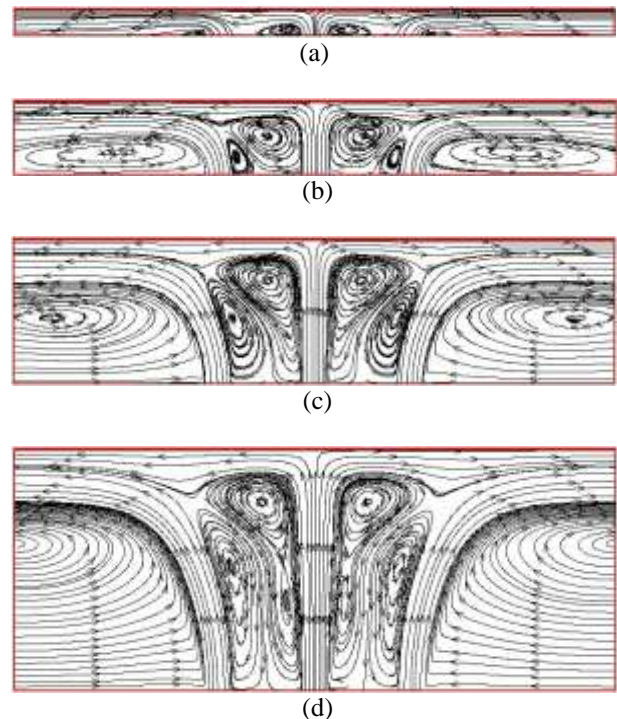


Figure 2. Streamline images obtained with Realizable $k-\epsilon$ turbulence model at $S/D=4$ and $Re=30000$ a) $H/D=1$ b) $H/D=3$ c) $H/D=6$ d) $H/D=10$.

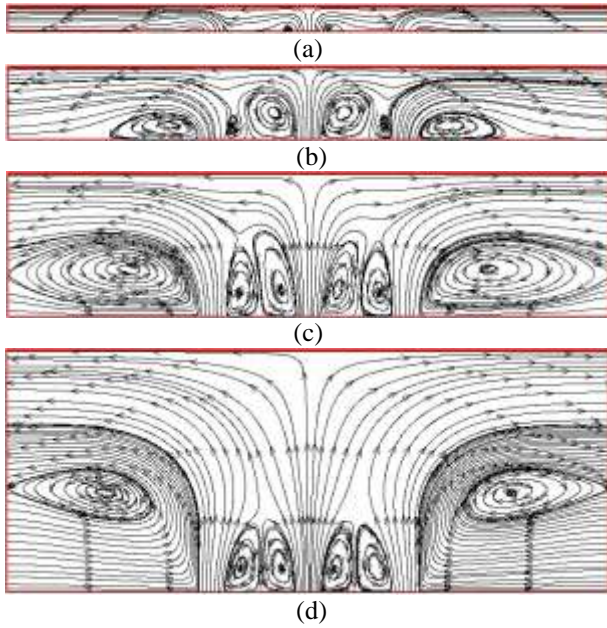


Figure 3. Streamline images obtained with Standard $k-\omega$ turbulence model at $S/D=4$ and $Re=30000$
a) $H/D=1$ b) $H/D=3$ c) $H/D=6$ d) $H/D=10$.

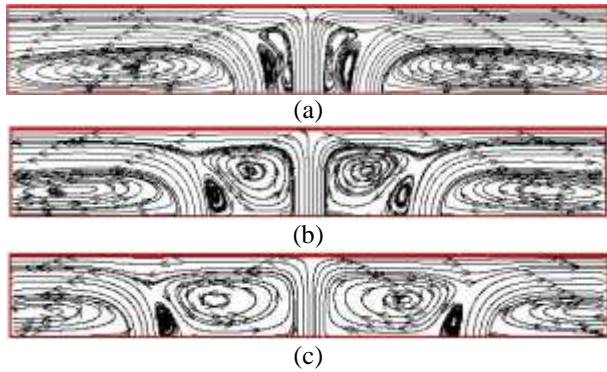


Figure 4. Streamline images obtained with Realizable $k-\epsilon$ turbulence model at $H/D=3$ and $Re=30000$
a) $S/D=2$ b) $S/D=4$ c) $S/D=6$.

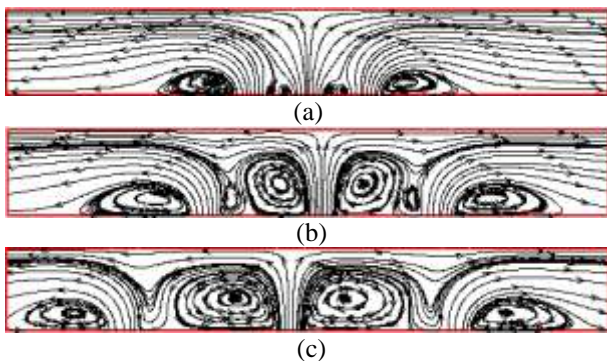


Figure 5. Streamline images obtained with Standard $k-\omega$ turbulence model at $H/D=3$ and $Re=30000$
a) $S/D=2$ b) $S/D=4$ c) $S/D=6$.

The effect of the nozzle-to-plate spacing (H/D) to the computed local pressure distributions on the impingement plate at $S/D=4$ and $Re=30000$ are shown in Figures 6a and b for Realizable $k-\epsilon$ and Standard $k-\omega$

turbulence models, respectively. It is seen from Figure 6a that subatmospheric regions occur on the impingement plate for nozzle-to-plate spacings up to 6. The subatmospheric regions become stronger with decreasing nozzle-to-plate spacing. Local pressure for $H/D=1$ starts sharply to decrease from the stagnation point of central jet with increasing radial distance (r/D) and reaches a minimum value and then increases to maximum value at the point of $r/D \sim \pm 3.1$ beyond which it starts sharply to decrease again until subatmospheric region within which it reaches a negative minimum value then restarts increasing towards the atmospheric value.

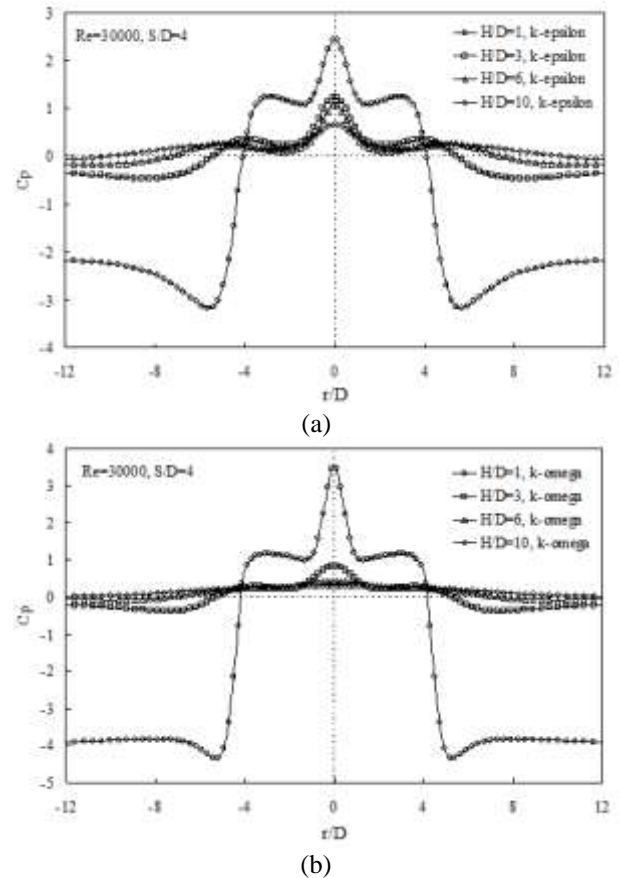


Figure 6. The effect of the nozzle-to-plate spacing on the computed pressure distributions for $Re=30000$ at $S/D=4$
a) Realizable $k-\epsilon$ turbulence model
b) Standard $k-\omega$ turbulence model.

As the nozzle-to-plate spacings increases, fluid velocity decreases due to jet spreading and the location at which local pressure becomes subatmospheric shifts to larger radial distance. The strength of subatmospheric region decreases with increasing H/D . The pressure gradient takes negative and positive values within this region. The positive pressure gradient separates the flow from the surface as found from the study of impinging air jets by Obot and Trabold (1987). The maximum values at the stagnation point of central jet decrease with increasing H/D spacings. This is because the kinetic energy at the jet center decreases due to jet spreading (Fattah, 2007). The maximum values at the stagnation point of central jet are greater than the maximum values

at the stagnation points of neighbor jet. This is because the central jet suppresses the neighbor jets. Local pressure distributions obtained with Standard $k-\omega$ model for the same parameters show similar behavior with the Realizable $k-\epsilon$ model results. However, pressure coefficients computed with Standard $k-\omega$ model have higher values (Figure 6b).

The effect of the jet-to-jet spacing (S/D) to the computed local pressure distributions on the impingement plate at $H/D=1$ and $Re=30000$ for Realizable $k-\epsilon$ and Standard $k-\omega$ turbulence models are shown in Figures 7a and b. It is seen from figures that as jet-to-jet spacing increases, the locations of stagnation points of neighbor jets and negative minimum values in subatmospheric regions shift to larger radial distances. Combining of the jets is late by increasing S/D and hence the intensity of the flow decreases (Fattah, 2007). Local pressure distributions computed with Standard $k-\omega$ turbulence model have the same trend with Realizable $k-\epsilon$ turbulence model's.

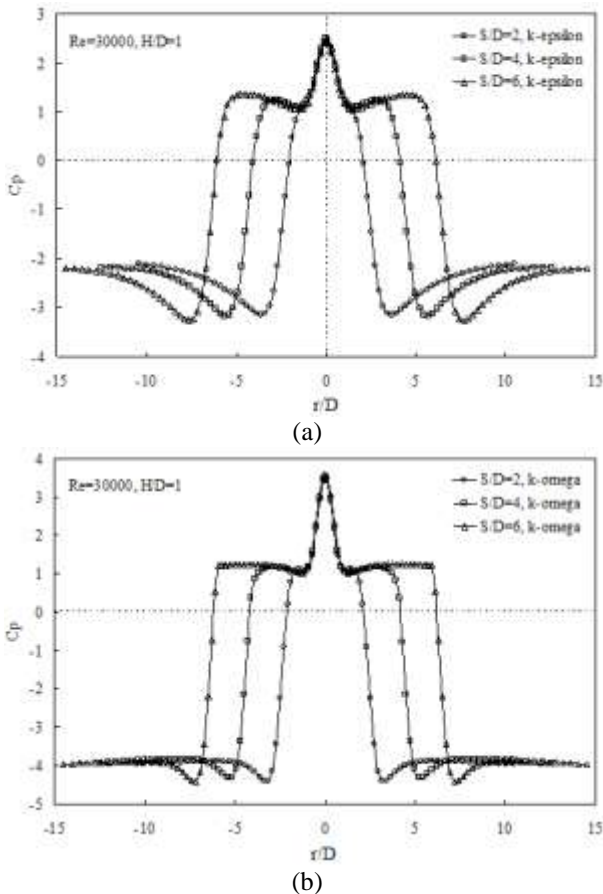


Figure 7. The effect of the jet-to-jet centerline spacing on the computed pressure distributions for $Re=30000$ at $H/D=1$
a) Realizable $k-\epsilon$ turbulence model
b) Standard $k-\omega$ turbulence model.

Heat Transfer

The effect of the nozzle-to-plate spacing (H/D) to the computed Nusselt number distributions on the impingement plate at $S/D=4$ and $Re=30000$ are shown

in Figures 8a and b for Realizable $k-\epsilon$ and Standard $k-\omega$ turbulence models, respectively.

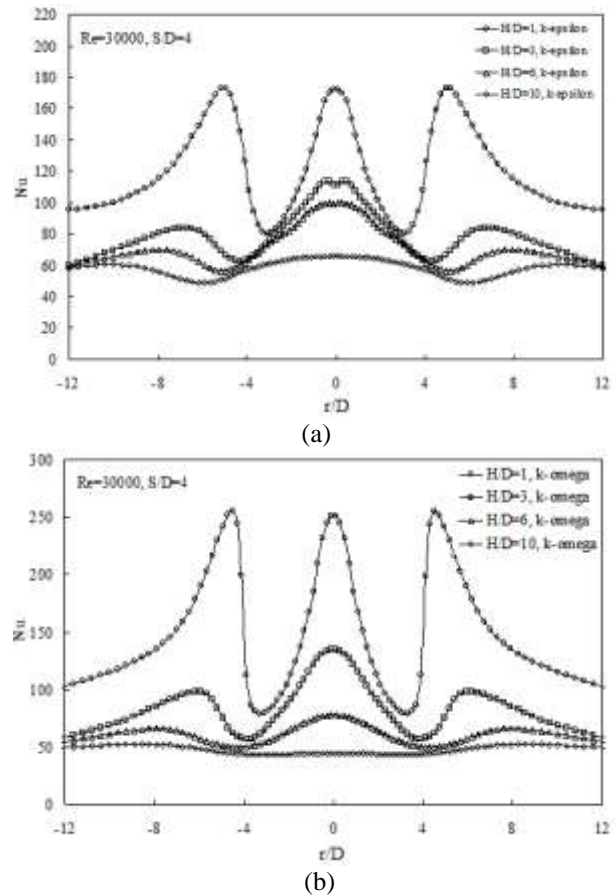


Figure 8. The effect of the nozzle-to-plate spacing on the computed local Nusselt number distributions for $Re=30000$ at $S/D=4$ a) Realizable $k-\epsilon$ turbulence model b) Standard $k-\omega$ turbulence model.

The local Nusselt number was defined as $Nu = h \cdot D / k_a$, where $h = q / (T_w - T_j)$ is convective heat transfer coefficient, T_w and T_j are the impingement wall and jet exit temperatures. It is observed from the figures that the influence of the nozzle-to-plate spacing on the Nusselt number distributions is very significant. Stagnation Nusselt numbers and heat transfer ratios increase as the nozzle-to-plate spacing decreases. Local Nusselt profiles computed with Realizable $k-\epsilon$ turbulence model have three peaks. (Figure 8a). While every three peaks have nearly the same value for $H/D=1$, Nusselt number peaks at the stagnation points of central jets are greater than the other Nusselt number peaks at larger H/D spacings. Secondary Nusselt number peaks shift to larger radial distance with increasing H/D spacings. The existence of the peaks in Nusselt number data is mainly explained with the transition from laminar to turbulent flow in wall jet region and increase of the wall-adjacent turbulence level as also mentioned in the study of Attalla and Specht (2009). The position of the maximum heat transfer depends on the flow from the adjacent nozzles and the distance between the nozzle and the impingement surface.

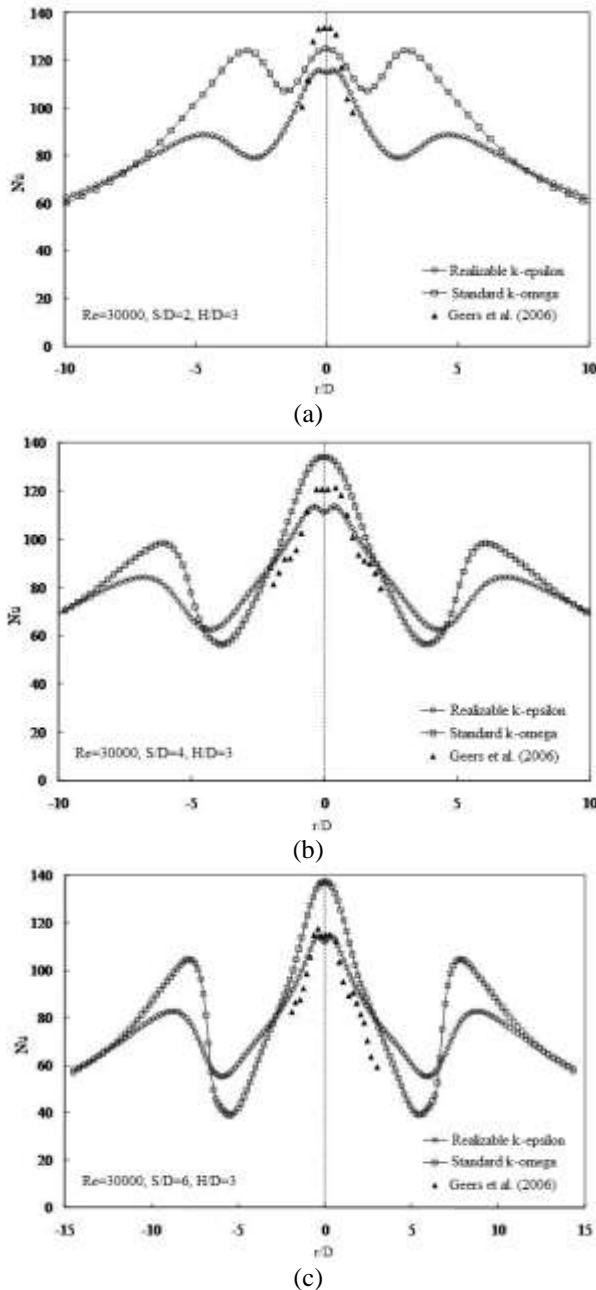


Figure 9. The comparison of computed Nusselt distributions on the impingement plate with experimental data for $Re=30000$ at $H/D=3$ a) $S/D=2$ b) $S/D=4$ c) $S/D=6$.

Local Nusselt number profiles obtained with Standard $k-\omega$ turbulence model for the same parameters show similar behavior with the Realizable $k-\epsilon$ model results (Figure 8b). The comparison between the distributions of Nusselt number and pressure coefficient obtained with the two turbulence models shows that the radial locations of minimum peaks of local Nusselt numbers are almost the same with the radial locations of maximum values of pressure coefficients. Beside this, at the radial distances where secondary peaks in Nusselt distributions occur, local pressures have negative minimum values in the subatmospheric regions. The magnitude of the Nusselt number is not affected by the jet-to-jet spacing and secondary peaks in Nusselt

number distributions shift to larger radial distances with increasing S/D .

The comparisons of heat transfer distributions computed with two turbulence models at present study and measured by Geers *et al.* (2006) at $Re=30000$ and $H/D=3$ for $S/D=2, 4$ and 6 are shown in Figures 9a, b and c respectively. It is seen from the figures that Standard $k-\omega$ model predicts greater local Nusselt numbers than Realizable $k-\epsilon$ model and the numerical results obtained using Realizable $k-\epsilon$ model are in better agreement with the experimental data. The accordance of Realizable $k-\epsilon$ model results with experiments increases as S/D increases.

CONCLUSION

A numerical investigation was carried out on the flow structure and heat transfer characteristics of a confined impinging jet array using two different turbulence models for Reynolds number of 30000 at the various nozzle-to-plate spacings and jet-to-jet spacings. Local pressure and heat transfer distributions on the impingement surface depend on nozzle-to-plate spacing while they are independent from jet-to-jet spacing. The magnitudes of the local pressure coefficients and Nusselt numbers decrease as the nozzle-to-plate spacing increases. Subatmospheric pressure regions occur on the impingement plate for nozzle-to-plate spacings up to 6. Nusselt number distributions show three maximum peaks. Jet array system enhances the local heat transfer in comparison with that of a single nozzle. Radial locations of minimum peaks of local Nusselt numbers are same with the radial locations of maximum values of pressure coefficients originating neighbor jets. At the radial distances where secondary peaks in Nusselt distributions occur, local pressures have negative minimum values in the subatmospheric regions. These relations show a linkage between the subatmospheric regions in pressure distribution and the peaks in heat transfer coefficients on the impingement surfaces. It is concluded from the two numerical simulations that Realizable $k-\epsilon$ turbulence model predicts the flow structures and heat transfer distributions more accurately than Standard $k-\omega$ turbulence model. The differences between numerical and experimental results can be explained with insufficiency of used turbulence models and the two dimensional computational domain. It is hoped that this study would provide data for the further research on this topic.

REFERENCES

- Abdel-Fattah A., 2007, Numerical and Experimental Study of Turbulent Impinging Twin Jet Flow, *Experimental Thermal and Fluid Science*, 31, 1060-1072.
- Aldabbagh L.B.Y. and Sezai I., 2002, Numerical Simulation of Three-Dimensional Laminar Multiple

- Impinging Square Jets, *International Journal of Heat and Fluid Flow*, 23, 509-518.
- Aldabbagh L.B.Y. and Sezai I., 2002, Numerical Simulation of Three-Dimensional Laminar, Square Twin-Jet Impingement on a Flat Plate, Flow Structure and Heat Transfer, *Numerical Heat Transfer, Part A*, 41, 835-850.
- Attalla M. and Specht E., 2009, Heat Transfer Characteristics from In-Line Arrays of Free Impinging Jets, *Heat and Mass Transfer*, 45, 537-543.
- Barata J.M.M., 1996, Fountain Flows Produced by Multiple Impinging Jets in a Cross Flow, *AIAA Journal*, 34, 2523-2530.
- Chuang S.H., Chen M.H., Lii S.W. and Tai F.M., 1992, Numerical Simulation of Twin-Jet Impingement on a Flat Plate Coupled with Cross Flow, *International Journal for Numerical Methods in Fluids*, 14, 459-475.
- Chuang S.H. and Nieh T.J., 2000, Numerical Simulation and Analysis of Three Dimensional Turbulent Impinging Square Twin Jet Flow Field with No-Cross Flow, *International Journal of Numerical Methods in Fluids*, 33, 475-498.
- Dagtekin I. and Oztop H.F., 2008, Heat Transfer due to Double Laminar Slot Jets Impingement on to an Isothermal Wall within one Side Closed Long Duct, *International Communications in Heat and Mass Transfer*, 35, 65-75.
- Fernandez J.A., Elicer-Cortes J.C., Valencia A., Pavagean M. and Gupta S., 2007, Comparison of Low Cost Two Equation Turbulence Models for Prediction Flow Dynamics in Twin Jet Devices, *International Communications in Heat and Mass Transfer*, 34, 570-578.
- Garrett K. and Webb B.W., 1999, The Effect of Drainage Configuration on Heat Transfer under an Impinging Liquid Jet Array, *ASME Journal of Heat Transfer*, 121, 803-810.
- Geers L.F.G., Hanjalic K. and Tummers M.J., 2006, Wall Imprint of Turbulence Structures and Heat Transfer in Multiple Impinging Jet Arrays, *Journal of Fluid Mechanics*, 546, 255-284.
- Hollworth B.R. and Berry R.D., 1978, Heat Transfer from Arrays of Impinging Jets with Large Jet-to-Jet Spacing, *J. Heat Transfer*, 100, 352-357.
- Hollworth B.R. and Dagan L., 1989, Arrays of Impinging Jets with Spent Fluid Removal through Vent Holes on the Target Surface-Part 1: Average Heat Transfer, *ASME J. Eng. Power*, 102, 994-999.
- Huber A.M. and Viskanta R., 1994, Effect of Jet-to-Jet Spacing on Convective Heat Transfer to Confined, Impinging Arrays of Axisymmetric Air Jets, *Int. J. Heat Mass Transfer*, 37, 2859-2869.
- Kim S.W. and Benson T.J., 1993, Fluid Flow of a Row of Jets in Cross-Flow - A Numerical Study, *AIAA Journal*, 31, 806-811.
- Koopman R.N. and Sparrow E.M., 1976, Local and Average Transfer Coefficients due to an Impinging Row of Jets, *Int. J. Heat Mass Transfer*, 19, 673-683.
- Koopman R.N., 1975, Local and Average Transfer Coefficients for Multiple Impinging Jets, Ph.D. Thesis, University of Minnesota.
- Kumar M.A. and Prasad B.V.S.S.S., 2011, Computational Flow and Heat Transfer of Multiple Circular Jets Impinging on a Flat Surface with Effusion, *Heat and Mass Transfer*, 47, 1121-1132.
- Martin H., 1977, Heat and Mass Transfer between Impinging Gas Jets and Solid Surfaces, *Adv. Heat Transfer*, 13, 1-60.
- Metzger D.E., Florschuetz L.W., Takeuchi D.I., Behee R.D. and Berry R.A., 1979, Heat Transfer Characteristic for Inline and Staggered Arrays of Circular Jets with Cross-Flow of Spent Air, *ASME Journal of Heat Transfer*, 101, 526-531.
- Miao J.M., Wu C.Y. and Chen P.H., Numerical Investigation of Confined Multiple Jet Impingement Cooling over a Flat Plate at Different Cross-Flow Orientations, *Numerical Heat Transfer, Part A*, 55, 1019-1050.
- Mikhail S., Morces S.M., Absu-Ellail M.M.M. and Ghaly W.S., 1982, Numerical Prediction of Flow Field and Heat Transfer from a Row of Laminar Slot Jets Impinging on a Flat Plate, *Heat Transfer*, 3, 377-382.
- Obot N.T and Trabold T.A., 1987, Impinging Heat Transfer within Arrays of Circular Jets: Part 1- Effects of Minimum, Intermediate and Complete Cross-Flow for Small and Large Spacings, *Journal of Heat Transfer*, 109, 872-879.
- Polat S., Huang B., Mujumdar A.S. and Douglas W.J.M., 1989, Numerical flow and heat transfer under Impinging Jets : A Review, *Ann. Rev. Numer. Fluid Mech. Heat Transfer*, 2, 157-197.
- Saad N.R., Polat S. and Douglas W.J.M., 1992, Confined Multiple Impinging Slot Jets without Cross-Flow Effects, *Int. Heat Fluid Flow*, 13, 2-14.
- Syedain S.H., Hasan M. and Mujumdar A.S., 1995, Turbulent Flow and Heat Transfer from Confined

Multiple Impinging Slot Jets, *Numerical Heat Transfer*, 18, 35-51.

Tanaka E., 1974, The Interference of two Dimensional Parallel Jets Experiments on the Combined Flow of Dual Jets, *Bull. ASME*, 17, 920-927.

Tzeng P.Y., Soong C.Y. and Hsieh C.D., 1999, Numerical Investigation of Heat Transfer under Confined Impinging Turbulent Slot Jets, *Numer. Heat Transfer, Part A*, 35, 903-924.

Yang Y. and Shyu C., 1998, Numerical Study of Multiple Impinging Slot Jets with an Inclined Confinement Surfaces, *Numerical Heat Transfer, Part A*, 33, 23-37.

Xing Y., Spring S. and Weigand B., 2010, Experimental and Numerical Investigation of Heat Transfer Characteristics of Inline and Staggered Arrays of Impinging Jets, *Journal of Heat Transfer*, 132, 1-11.